HYBRID ELECTRIC VEHICLES

UNIT-5

INTRODUCTION:

TABLE 3.1 Nominal Energy Density of Sources

Energy Source	Nominal Specific Energy (Wh/kg)
Gasoline	12,500
Natural gas	9350
Methanol	6050
Hydrogen	33,000
Coal (bituminous)	8200
Lead-acid battery	35
Lithium-polymer battery	200
Flywheel (carbon-fiber)	200

ESS: ELECTRICAL ENERGY STORAGE:

Critical measures of an ESS performance are

1. Safety: Ensure safe operation of ESS, no risk of thermal runaway, or exothermic behavior in the event of a crash or short circuit.
2. Cycle life: The number of full charge/discharge cycles until the ESS reaches end-of-life (EOL) condition; the definition of EOL condition varies with the usage of the ESS. One commonly used EOL condition is battery's remaining capacity at 80% of its beginning-of-life (BOL) capacity.
3. Calendar life: The calendar longevity of the ESS when it is at storage (month or year).
4. Energy density: The amount of energy each kilogram or liter of ESS contains (Wh/kg and Wh/L).
5. Power density: The amount of power each kilogram or liter of ESS delivers per second (W/kg and W/L).
6. Charge acceptance capacity: The amount of energy the ESS absorbs per second (W/kg and W/L).
7. Cost: $ per kWh.

The ultimate goal for ESS performance would be to offer similar energy and power densities to petroleum fuels used in conventional vehicles, with a comparable cost of an IC engine. However, this is not feasible with the current technology and a compromise has to be made.

TABLE 7.3

Comparison of Electrical Energy Storage Technologies

	Lead Acid	NiMH	Li-ion	Na–Ni–Cl	EDLC	Hybrid UC
Specific energy (Wh/kg)	30–50	60–120	100–265	100–120	2.5–15	2.84–120
Energy density (Wh/L)	50–80	140–300	250–730	150–180	10–30	5.6–140
Specific power (W/kg)	75–300	250–1000	250–340	150–200	500–5000	2300–14,000
Power density (W/L)	10–400	80–300	100–210	220–300	100,000	2500–27,000
Round-trip efficiency (%)	70–80	60–70	85–98	85–90	90–98	95–99
Self-discharge (%/day)	0.033–0.3	25–30	0.1–0.3	15	20–40	0.1–12.5
Cycle lifetime (cycles)	100–2000	500–1000	400–1200	2500	10,000–100,000	5000–200,000
Power capacity Cost ($/kW)	175–600	150–1500	175–4000	150–300	100–360	50–320
Energy capacity Cost ($/kWh)	150–400	150–1500	500–2500	100–200	300–94,000	600–50,000

Source: Augmented from Bradbury, K. *Energy Storage Technology Review*. Duke University, Durham, NC, 2010: 1–34.

7.5 CHARACTERISTIC TERMINOLOGY AND PERFORMANCE PARAMETERS

Specific energy	Energy per unit mass, typically expressed as Wh/kg
Energy density	Energy per unit volume, typically expressed as Wh/L
Specific power	Power per unit mass, typically expressed as W/kg
Power density	Power per unit volume, typically expressed as W/L
Round-trip efficiency	Expressed as percentage of fraction of energy output during discharge compared to input energy during charge
Self-discharge	Energy loss per unit time, typically %/day
Cycle lifetime	Expected number of useful cycles, dependent on definition of cycle
Power capacity cost	Monetary cost per unit power, for example, $/kW
Energy capacity cost	Monetary cost per unit energy, for example, $/kWh
SOC	Either expressed as a percentage 0%–100% or number between 0 and 1. Indicates the recommended extremes of cell states, for example, active-material/ion concentrations in an electrochemical cell, which represent a fully charged or fully discharged cell condition. Typical definitions of SOC involve integrating current flow and dividing by the rated capacity.
DOD	Indicates the ratio or percentage to the total capacity that has been discharged, for example, DOD = 1 − SOC or DOD% = 100 − SOC%.
Ampere hour (Ah) capacity	A common unit manufacturers use to describe the total capacity of a cell under some predescribed conditions, for example, 20°C at 1/20 C discharge rate. A related metric is watt-hour (Wh) obtained by multiplying rated Ah by rated cell voltage.
Discharge capacity	The total capacity that can be extracted from a fully charged cell from SOC = 1 to SOC = 0. Denoted as Ah_d or Wh_d.
Charge capacity	The total capacity that can be charged into a cell from SOC = 0 to SOC = 1. Denoted as Ah_c or Wh_c.
Coulombic efficiency	Also called Faradaic efficiency for an electrochemical cell, it describes the efficiency in which charge (e.g., electrons) is transferred in a system to facilitate the main electrochemical reaction. Participation in side reactions generating heat is an example of Faradaic loss. Separate efficiencies for charging and discharging are possible. The metric is typically measured stoichiometrically by comparing transferred charge to amounts of active material.
C-rate	A charge or discharge rate equal to the rate that can fully charge or discharge the cell in 1 h.
Min/max cutoff voltage	Manufacturer-specified voltages limit the cell. Current limitations need to be applied to avoid exceeding these limits.
Calendar life	The expected life span of the cell under storage conditions. Can be sensitive to factors such as ambient temperature and SOC.
Cell voltage reversal	Weak cells forcibly operated at negative voltages can result in a possibly permanent, polarity reversal at the cell terminals. Can shorten cell life or lead to complete failure.

Remaining useful life (RUL)	Typically, a unit of time representing the remaining life of the cell before it no longer satisfies application requirements of power output and available capacity. It is heavily dependent on operating conditions such as environmental factors and usage history.
State of health (SOH)	A dimensionless metric used to define the general health or usability of the cell usually for the purpose of estimating RUL. Impedance-based metrics, for example, SOH_r, are typically defined based on ratios of the aged cell impedance and fresh cell impedance. Capacity-based SOH, for example, SOH_c, is based on ratios of aged cell-degraded capacity and fresh cell capacity. Many variations of SOH equations are possible.
BMS	The BMS is a combination of battery pack hardware and software with measurement, control, and communication capabilities to report the status/states of the multiple cells and perform low-level protection features such as cell balancing, thermal management, and optimal cell control.
Battery state estimation (BSE)	A collection of algorithms and software residing in the BMS to perform key functions such as estimating SOC, SOH, RUL, capacity, and maximum available power output.
Open-circuit voltage (OCV)	An internal voltage of the cell that is measured across the cell terminals in zero-current/disconnected rested equilibrium conditions. Its value is dependent on cell SOC and hysteresis effects.
Electrochemical impedance spectroscopy (EIS)	A frequency domain-testing procedure employing small signal input perturbations at common cell-operating points.
Potentiostatic	A term to describe an EIS testing condition where the average input signal is a constant voltage (CV) and output is the current response.
Galvanostatic	A term to describe an EIS testing condition where the average input signal is a constant current (CC) and output is the voltage response.
ESR	Typically related to the series resistance to represent losses in inductors/capacitors.
ECM	Equivalent circuit model

TABLE 3.5 Properties of EV and HEV Batteries

Battery Type	Specific Energy, Wh/kg	Specific Power, W/kg	Energy Efficiency, %	Cycle Life	Estimated Cost, US$/*kWh*
Lead-acid	35–50	150–400	80	500–1000	100–150
Nickel-cadmium	30–50	100–150	75	1000–2000	250–350
Nickel-metal-hydride	60–80	200–300	70	1000–2000	200–350
Aluminum-air	200–300	100	<50	Not available	Not available
Zinc-air	100–220	30–80	60	500	90–120
Sodium-sulfur	150–240	230	85	1000	200–350
Sodium-nickel-chloride	90–120	130–160	80	1000	250–350
Lithium-polymer	150–200	350	Not available	1000	150
Lithium-ion	80–130	200–300	>95	1000	200

1.Energy Storage - Battery based energy storage and simplified models of battery:

The major types of rechargeable batteries considered for EV and HEV applications are:

- Lead-acid (Pb-acid)
- Nickel-cadmium (NiCd)
- Nickel-metal-hydride (NiMH)
- Lithium-ion (Li-ion)
- Lithium-polymer (Li-poly)
- Sodium-sulfur (NaS)
- Zinc-air (Zn-Air)

CELL DISCHARGE OPERATION

In the cell discharge operation (Figure 3.2), electrons are consumed at the positive electrode, the supply of which comes from the negative electrode. The current flow is, therefore, out of the positive electrode into the motor-load, with the battery acting as the source.

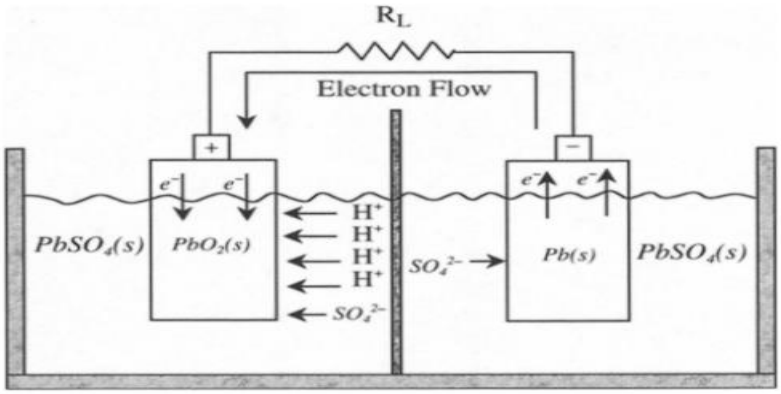

FIGURE 3.2 Lead-acid battery: cell discharge operation.

The positive electrode equation is given by:

$$PbO_2(s) + 4H^+(aq) + SO_4^{2-}(aq) + 2e \rightarrow PbSO_4 + 2H_2O(l)$$

A highly porous structure is used for the positive electrode to increase the PbO_2 (s)/electrolyte contact area, which is about 50 to 150 m^2 per Ah of battery capacity. This results in higher current densities, as PbO_2 is converted to $PbSO_4$ (s). As discharge proceeds, the internal resistance of the cell rises due to $PbSO_4$ formation and decreases the electrolyte conductivity as H_2SO_4 is consumed. $PbSO_4$(s) deposited on either electrode in a dense, fine-grain form can lead to sulfatation. The discharge reaction is largely inhibited by the buildup of $PbSO_4$, which reduces cell capacity significantly from the theoretical capacity.

The negative electrode equation during cell discharge is:

$$Pb(s) + SO_4^{2-}(aq) \rightarrow PbSO_4 + 2e$$

The electrons are released at the negative electrode during discharge operation. The production of PbSO4(s) can degrade battery performance by making the negative electrode more passive.

The overall cell discharge chemical reaction is:

$$Pb(s) + PbO_2(s) + 2H_2SO_4(aq) \rightarrow 2PbSO_4 + 2H_2O(l)$$

CELL CHARGE OPERATION

The cell charge operation (Figure 3.3) is the reverse of the cell discharge operation. During cell charging, lead sulfate is converted back to the reactant states of lead and lead oxide. The electrons are consumed from the external source at the negative electrode, while the positive electrode releases the electrons. The current flows into the positive electrode from the external source thereby delivering electrical energy into the cell, where it gets converted into chemical energy. The chemical reaction at the positive electrode during cell charging is:

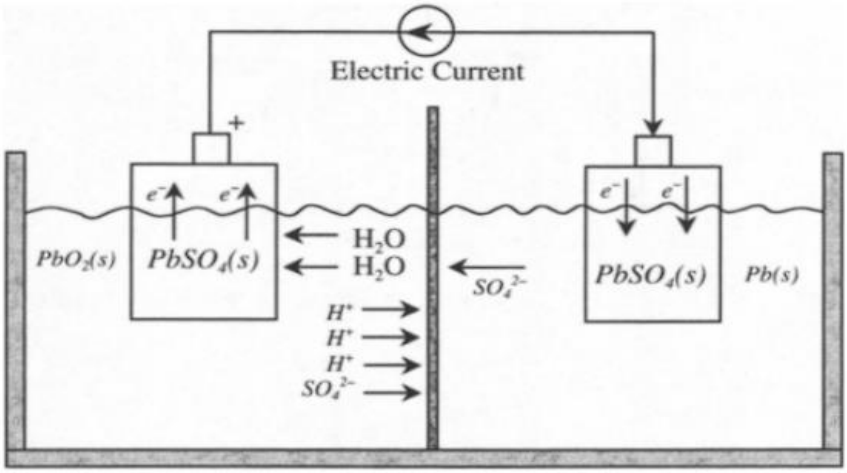

FIGURE 3.3 Lead-acid battery: cell charge operation.

$$PbSO_4(s) + 2H_2O(l) \rightarrow PbO_2(s) + 4H^+(aq) + SO_4^{2-}(aq) + 2e$$

The chemical reaction at the negative electrode during cell charging is:

$$PbSO_4(s) + 2e \rightarrow Pb(s) + SO_4^{2-}(aq)$$

The overall chemical reaction during cell charging is:

$$2PbSO_4(s) + 2H_2O(l) \rightarrow Pb(s) + PbO_2(s) + 2H_2SO_4(aq)$$

Conventionally, lead-acid batteries are of flooded-electrolyte cells, where free acid covers all the plates. This imposes the constraint of maintaining an upright position for the battery, which is difficult in certain portable situations. Efforts in developing hermetically sealed batteries faced the problem of buildup of an explosive mixture of hydrogen and oxygen on approaching the top-of-charge or overcharge condition during cell recharging. The problem is addressed in the valve-regulated-lead-acid (VRLA) batteries by providing a path for the oxygen, liberated at the positive electrode, to reach the negative electrode, where it recombines to form lead-sulfate. There are two mechanisms for making sealed VRLA batteries, the gel battery, and the AGM (absorptive glass microfiber) battery. These types are based on immobilizing the sulfuric acid electrolyte in the separator and the active materials, leaving sufficient porosity for the oxygen to diffuse through the separator to the negative plate.[1]

3.2.3 CONSTRUCTION

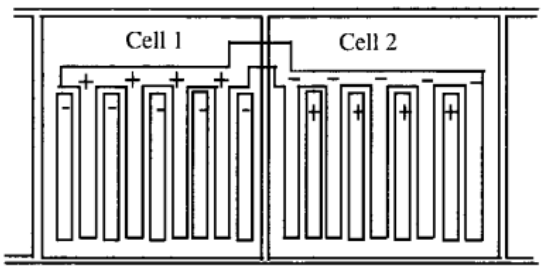

FIGURE 3.4 Schematic diagram of a lead-acid battery showing through-partition connection.

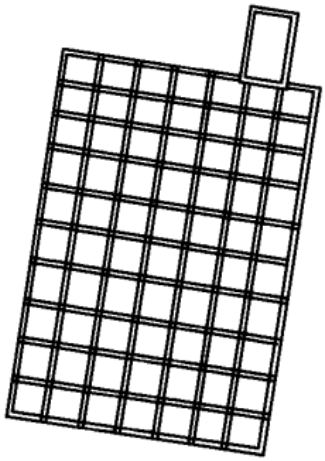

FIGURE 3.5 A lead-acid battery grid.

Construction of a typical battery consists of positive and negative electrode groups (elements) interleaved to form a cell. The through partition connection in the battery is illustrated in Figure 3.4. The positive plate is made of stiff paste of the active material on a lattice-type grid, which is shown in Figure 3.5. The grid, made of a suitably selected lead alloy, is the framework of a portable battery to hold the active material. The positive plates can be configured in flat pasted or tubular fashion. The negative plates are always manufactured as pasted types.

LI-ION BATTERY

Lithium metal has high electrochemical reduction potential (3.045 V) and the lowest atomic mass (6.94), which shows promise for a battery of 3 V cell potential when combined with a suitable positive electrode. The interest in secondary lithium cells soared soon after the advent of lithium primary cells in the 1970s, but the major difficulty was the highly reactive nature of the lithium metal with moisture, restricting the use of liquid electrolytes. Discovery in the late 1970s by researchers at Oxford University that lithium can be intercalated (absorbed) into the crystal lattice of cobalt or nickel to form $LiCoO_2$ or $LiNiO_2$ paved the way toward the development of Li-ion batteries.[3] The use of metallic-lithium is bypassed in Li-ion batteries by using lithium intercalated (absorbed) carbons (Li_xC) in the form of graphite or coke as the negative electrode, along with the lithium metallic oxides as the positive electrode. The graphite is capable of hosting lithium up to a composition of LiC_6. The majority of the Li-ion batteries uses positive electrodes of cobalt oxide, which is expensive but proven to be the most satisfactory. The alternative positive electrode is based on nickel oxide $LiNiO_2$, which is structurally more complex but costs less. Performance is similar to that of cobalt oxide electrodes. Manganese-oxide-based positive electrodes ($LiMn_2O_4$ or $LiMnO_2$) are also under research, because manganese is cheaper, widely available, and less toxic.

The cell discharge operation in a lithium ion cell using $LiCoO_2$ is illustrated in Figure 3.6. During cell discharge, lithium ions (Li^+) are released from the negative electrode that travels through an organic electrolyte toward the positive electrode. In the positive electrode, the lithium ions are quickly incorporated into the lithium compound material. The process is completely reversible. The chemical reactions at the electrodes are as follows:

At the negative electrode,

$$Li_xC_6 \underset{\text{Charge}}{\overset{\text{Discharge}}{\rightleftarrows}} 6C + xLi^+ + xe^- \quad \text{where } 0 < x < 1$$

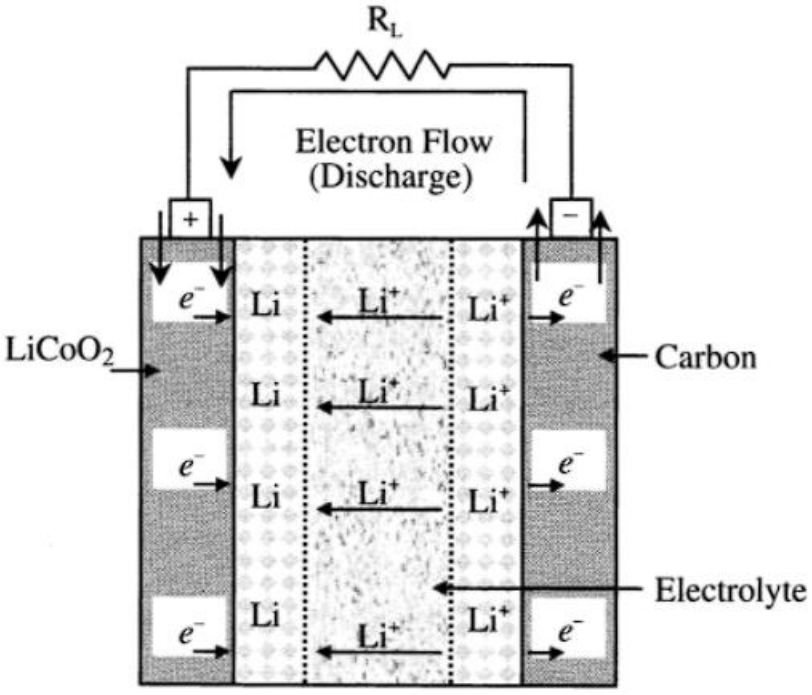

FIGURE 3.6 Lithium-ion cell.

At the positive electrode,

$$xLi^+ + xe^- + Li_{(1-x)}CoO_2 \underset{\text{Charge}}{\overset{\text{Discharge}}{\rightleftarrows}} LiCoO_2$$

During cell charge operation, lithium ions move in the opposite direction from the positive electrode to the negative electrode. The nominal cell voltage for a Li-ion battery is 3.6 V, which is equivalent to three NiMH or NiCd battery cells.

Lithium-ion batteries have high specific energy, high specific power, high energy efficiency, good high-temperature performance, and low self-discharge. The components of Li-ion batteries are also recyclable. These characteristics make Li-ion batteries highly suitable for EV and HEV and other applications of rechargeable batteries.

7.6.1 Electrochemical Cell—Equivalent Circuit Model

There are a variety of ECM approaches and topologies for electrochemical cells. They typically contain common circuit elements to mimic the experimental responses observed from cell characterization data. In this section, a specific ECM with n RC elements, depicted in Figure 7.17, is presented that mimics effects such as transient response, hysteresis, nonlinear OCV, asymmetric internal resistance, and thermal dependence. It can be readily modeled in circuit simulation software using standard packages such as PLECS and/or Matlab Simscape/SimPowerSystems.

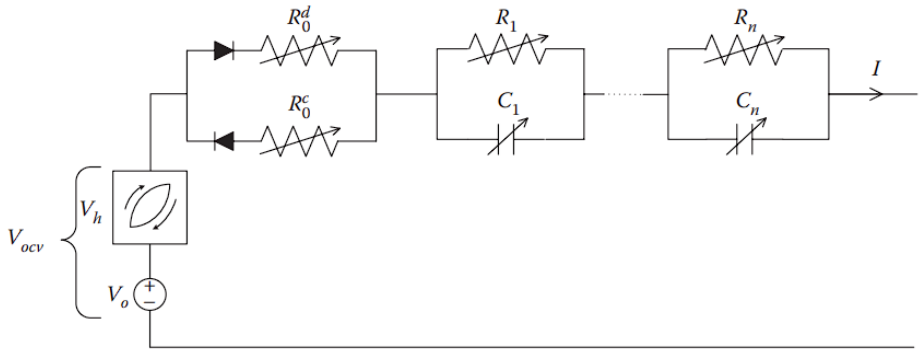

FIGURE 7.17 Equivalent circuit model of battery cell.

3.7
BATTERY MODELING

Peukert's equation is a widely accepted empirical relation among capacity *(Q)*, discharge current *(I)*, and time *(t)* or among specific power *(SP)*, specific energy *(SE)*, and time *(t)*. Peukert's equation is used in developing a *fractional depletiont model* (FDM) of batteries. The FDM of a battery can be used to predict the range of an EV. The FDM can be developed using the constant current discharge approach or the power density approach associated with the two forms of Peukert's equation.

3.7.1
CONSTANT CURRENT DISCHARGE APPROACH

Consider the constant current discharge experiment of Figure 3.13. The battery is discharged under constant current condition from 100% capacity until cut-off voltage is reached. The load resistance R_L is varied to change the constant current level and also to maintain the current constant for each experiment. The I vs. t_{cut} data are used to fit Peukert's equation (Equation 3.9) with constant current:

$$I^n * t_{cut} = \lambda \tag{3.16}$$

where I is the constant discharge current; and λ, and n are curve-fitting constants, with $n \rightarrow 1$ for small currents and $n \rightarrow 2$ for large currents.

3.7.1.1
Fractional Depletion Model

Using Peukert's equation, we can establish the relationship between Q and I. The practical capacity of a battery is

$$Q = I * t_{cut}$$

$$\Rightarrow t_{cut} = \frac{Q}{I}$$

Substituting into Peukert's equation:

$$I^n\left(\frac{Q}{I}\right) = \lambda$$

$$\Rightarrow Q = \frac{\lambda}{I^{n-1}}$$

Because $0<n-1<1$, for $I>1$, Q decreases as I increases.

From Section 3.4, we know that

$$SoD = \int i(\tau)d\tau$$

and

$$DoD = \frac{SoD}{Q(i)}$$

SoD is the amount of charge that the battery generates to the circuit. Assume that at $t=t_0$, the battery is fully charged. Let us consider a small interval of time dt. Therefore,

$$d(DoD) = \frac{d(SoD)}{Q(i)}$$

where

$$d(SoD) = i(t)dt$$

We know that $Q=\lambda/I^{n-1}$ for constant current discharge. Let $Q=\lambda/i^{n-1}$ for time varying current as well, for lack of anything better.

Therefore,

$$d(DoD) = \frac{idt}{\lambda/i^{n-1}} = \frac{i^n}{\lambda}dt$$

Integrating, we obtain,

$$\int_{t_0}^{t} d(DoD) = \int_{t_0}^{t} \frac{i^n}{\lambda}dt$$

$$\Rightarrow DoD(t) - DoD(t_0) = \int_{t_0}^{t} \frac{i^n}{\lambda}dt$$

$DoD(t_0)=0$ if the battery is fully charged at $t=t_0$.

The *fractional depletion model* (FDM) is thus obtained as

$$DoD(t) = \left[\int_{t_0}^{t} \frac{i^n}{\lambda}dt\right] * 100\% \qquad (3.17)$$

The FDM based on current discharge requires knowledge of the discharge current $i(t)$. Therefore, this model to predict the EV range should be used when $i(t)$ is known.

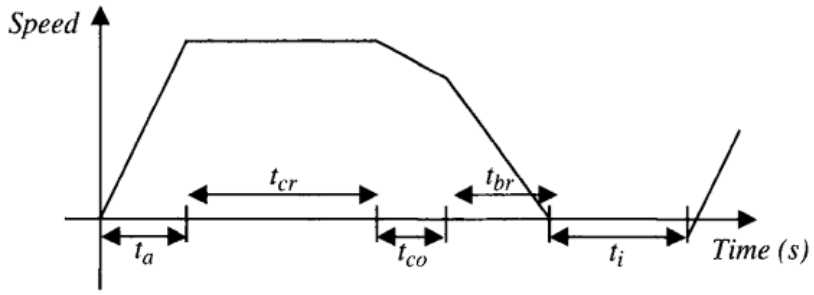

FIGURE 3.20 SAE J227a standard driving cycle.

3.7.2
STANDARD DRIVING CYCLES

The standard J227a driving cycle recommended by the Society of Automotive Engineers (SAE) is routinely used to evaluate the performance of EVs and energy sources. The SAE J227a has three schedules designed to simulate the typical driving patterns of fixed-route urban, variable-route urban, and variable-route suburban travels. These three patterns are the SAE J227a driving schedules B, C, and D, respectively. Each schedule has five segments in the total driving period:

1. Acceleration time t_a to reach the maximum velocity from start-up
2. Cruise time t_{cr} at a constant speed
3. Coast time t_{co} when no energy is drawn from the source
4. Brake time t_{br} to bring the vehicle to stop
5. Idle time t_i prior to the completion of the period

The driving cycle for J227a is shown in Figure 3.20, with the recommended times for each of the schedules given in Table 3.6. The figure drawn is slightly modified from the pattern recommended by the SAE. The J227a procedures specify only the cruise velocity and the time of transition from one mode to the other. The velocity profile at segments other than the cruising part is not fixed, and hence, the distance traversed during these other periods is also variable. In reality, the distances would depend on the design of the vehicle under consideration. For simplicity, straight-line approximations have been assumed in these schedules in this book.

3.7.3
POWER DENSITY APPROACH

Given a battery terminal power profile $p(t)$, the specific power $SP(t)$ profile can be obtained by dividing the power profile $p(t)$ by the total vehicle mass M_v. The battery is assumed to be fully charged at t=0. *Let* $f_y(t)$ be equal to the fraction of available energy provided by the battery from 0 to t, where $f_r(0)$=0, because SoD (0)=0. Now, consider the time interval dt over which a fraction of available energy df_r is provided by the battery:

$$df_r = \frac{dE}{E_{avail}} = \frac{\frac{dE}{M_v}}{\frac{dE_{avail}}{M_v}} = \frac{d(SE)}{SE_{avail}}$$

If dE is the energy provided by the battery to the electrical circuit over dt, and E_{avail} is the total available energy, then

$$dE = pdt$$

Now E_{avail} is a function of instantaneous power, and we know that

$$d(SE) = (SP)dt$$

Therefore,

$$SE_{avail} = f(SP)$$

We will use Peukert's equation to relate specific power and specific energy as follows:

$$(SP)^n * SE_{avail} = \lambda$$

Therefore,

$$df_r = \frac{SP}{\frac{\lambda}{(SP)^n}}\, dt = \frac{(SP)^{n+1}}{\lambda}\, dt$$

Integrating,

$$\int_{f_r(0)}^{f_r(t)} df_r = \int_0^t \frac{(SP)^{n+1}}{\lambda} d\tau$$

$$\Rightarrow f_r(t) = \int_0^t \frac{(SP)^{n+1}}{\lambda} d\tau \qquad (3.19)$$

Equation 3.19 is the FDM using the power density approach. If t is the time at which x% of available energy has been used, then

$$\frac{x}{100} = \int_0^t \frac{(SP)^{n+1}}{\lambda} d\tau$$

Note that

$$1 = \int_0^{t_{100\%}} \frac{(SP)^{n+1}}{\lambda} d\tau$$

At $t_{100\%}$, 100%, all of the available energy has been used by the system.

2.Fuel cells - their characteristics and simplified models:

4.1.1
FUEL CELL CHARACTERISTICS

Theoretically, fuel cells operate isothermally, meaning that all free energy in a fuel cell chemical reaction should convert into electrical energy. The hydrogen "fuel" in the fuel cell does not burn as in IC engines, bypassing the thermal to mechanical conversion. Also, because the operation is isothermal, the efficiency of such direct electrochemical converters is not subject to the limitation of Carnot cycle efficiency imposed on heat engines. The fuel cell converts the Gibbs free energy of a chemical reaction into electrical energy in the form of electrons under isothermal conditions. The maximum electrical energy for a fuel cell operating at constant temperature and pressure is given by the change in Gibbs free energy:

$$W_{el} = -\Delta G = nFE \tag{4.1}$$

where n is the number of electrons produced by the anode reaction; F is Faraday's constant, equal to 96412.2 C/mol; and E is the reversible potential. The Gibbs free energy change for the reaction $H_2(g)+(1/2)O_2(g)\rightarrow H_2O(l)$ at standard condition of 1 atmospheric pressure and 25°C is −236 kJ/mol or −118 MJ/kg. With n=2, the maximum reversible potential under the same conditions is E_0=1.23 V, using Equation 4.1. The maximum reversible potential under actual operating conditions for the hydrogen-oxygen fuel cell is given by the Nernst equation, as follows:[1]

$$E = E_0 + \left(\frac{RT}{nF}\right)\ln\left[\frac{P_H \cdot P_O^{1/2}}{P_{H_2O}}\right] \tag{4.2}$$

where T is the temperature in Kelvin; R is the gas constant; and P_H, P_o, and P_{H_2O} are the concentrations or partial pressures of the reactants and products.

The voltage-current output characteristic of a hydrogen-oxygen cell is illustrated in Figure 4.2. The higher potentials around 1 V per cell are theoretical predictions that are not achievable in a practical cell. The linear region where the reduction in cell potential is due to ohmic losses is where a practical fuel cell operates. The resistive components in the cell limit the practical achievable efficiency of a fuel cell. The working voltage of the cell falls with an increasing current drain, knowledge that is important in designing fuel-cell-powered EVs and hybrid vehicles. Because cell potential is small, several cells are stacked in series to achieve the desired voltage. The major advantage of fuel cells is lower sensitivity to scaling, which means that fuel cells in the kW range have similar overall system efficiencies up to the MW range.

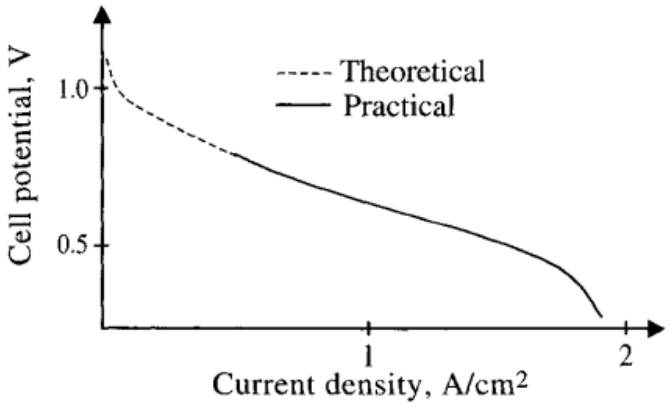

FIGURE 4.2 Voltage-current relationship of a hydrogen/oxygen cell.

4.1.2 FUEL CELL TYPES

The six major types of fuel cells are as follows: alkaline, proton exchange membrane, direct methanol, phosphoric acid, molten carbonate, and solid oxide. A short description of the relevant characteristics of each type in the context of vehicular and stationary applications is given below.[2,3]

4.1.2.1 Alkaline Fuel Cell (AFC)

In an alkaline fuel cell (AFC), an aqueous solution of potassium hydroxide (KOH) is used as the electrolyte. Compared to some other fuel cells where acidic electrolytes are used, the performance of the alkaline electrolyte is as good as the acid electrolytes, while being significantly less corrosive toward the electrodes. Alkaline fuel cells have been in actual use for a long time, delivering electrical efficiencies of up to 60%. They require pure hydrogen as fuel and operate at low temperatures (at 80°C); therefore, they are suitable for vehicle applications. Residual heat can be used for heating, but the cell temperature is not sufficiently high to generate steam that can be used for cogeneration.

4.1.2.2 Proton Exchange Membrane (PEM)

The proton exchange membrane (PEM) fuel cells use solid electrolytes and operate at low temperatures (around 80°C). Nafion is an example of solid polymer electrolyte. These fuel cells are also known as solid polymer membrane fuel cells. The electrical efficiency of PEM fuel cells is lower than that of the alkaline cells (about 40%). However, a rugged and simple construction makes these types of fuel cells suitable for vehicle applications. The PEM fuel cell and the AFC are currently being considered for vehicle applications. The advantage

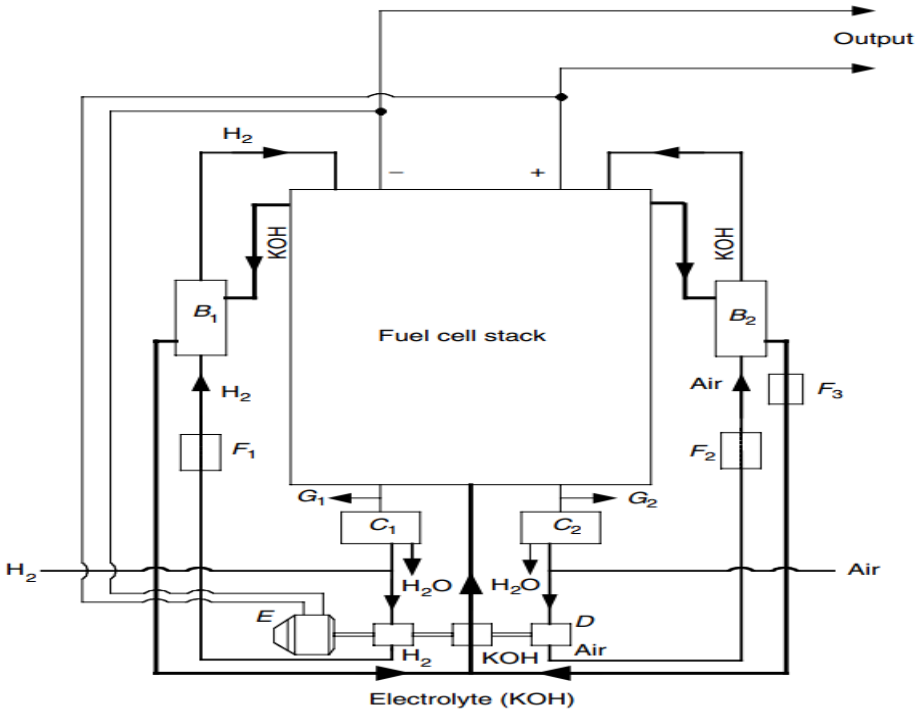

FIGURE 12.7
Circulating electrolyte and supplies of hydrogen and air in an AFC: B_1, B_2, heater exchangers; C_1, C_2, condensers; D, pampers; E, motor; F_1, F_2, F_3, controls; G_1, G_2, outlets[1]

figure 12.7 Alkaline Fuel Cell

of PEM cells is that they can tolerate impurity in the fuel, as compared to pure hydrogen which is needed in alkaline fuel cells.

4.1.2.3
Direct Methanol Fuel Cell (DMFC)

The direct methanol fuel cell (DMFC) is a result of research on using methanol as the fuel that can be carried on-board a vehicle and reformed to supply hydrogen to the fuel cell. A DMFC works on the same principle as the PEM, except that the temperature is increased to the range of 90 to 120°C such that internal reformation of methanol into hydrogen is possible. The electrical efficiency of DMFC is quite low at about 30%. This type of fuel cell is still in the design stages, because the search for a good electrocatalyst to reform the methanol efficiently and to reduce oxygen in the presence of methanol is ongoing.

4.1.2.4
Phosphoric Acid Fuel Cell (PAFC)

Phosphoric acid fuel cells (PAFC) are the oldest type with an origin that extends back to the creation of the fuel cell concept. The electrolyte used is phosphoric acid, and the cell operating temperature is about 200°C, which makes some cogeneration possible. The electrical efficiency of this cell is reasonable at about 40%. These types of fuel cells are considered too bulky for transportation applications, while higher efficiency designs exist for stationary applications.

4.1.2.5
Molten Carbonate Fuel Cell (MCFC)

Molten carbonate fuel cells, originally developed to operate directly from coal, operate at 600°C and require CO or CO_2 on the cathode side and hydrogen on the anode. The cells use carbonate as the electrolyte. The electrical efficiency of these fuel cells is high at about 50%, but the excess heat can be used for cogeneration for improved efficiency. The high temperatures required make these fuel cells not particularly suitable for vehicular applications, but they can be used for stationary power generation.

4.1.2.6
Solid Oxide Fuel Cell (SOFC, ITSOFC)

Solid oxide fuel cells (SOFCs) use a solid ionic conductor as the electrolyte rather than a solution or a polymer, which reduces corrosion problems. However, to achieve adequate ionic conductivity in such a ceramic, the system must operate at very high temperatures. The original designs, using yttria-stabilized zirconia as the electrolyte, required temperatures as high as 1000°C to operate, but the search for materials capable of serving as the electrolyte at lower temperatures resulted in the "intermediate temperature solid oxide fuel cell" (ITSOFC). This fuel cell has high electrical efficiency of 50 to 60%, and residual heat can also be used for cogeneration. Although not a good choice for vehicle applications, it is at present the best option for stationary power generation.

The fuel cell features described above are summarized in Table 4.1. The usable energy and relative costs of various fuels used in fuel cells are listed in Table 4.2. The selection of fuel cells as the primary energy source in EVs and HEVs depends on a number of issues, ranging from fuel cell technology to infrastructure to support the system. Based on the discussion in this section, the choice of fuel cell for the vehicular application is an alkaline or proton exchange design, while for stationary applications, it will be the SOFC. The size, cost, efficiency, and start-up transient times of fuel cells are yet to be at an acceptable stage for EV and HEV applications. The complexity of the controller required for fuel cell operation is another aspect that needs further attention. Although its viability has been well-proven in the space program, as well as in prototype vehicles, its immature status makes it a longer-term enabling technology for an EV and HEV.

3.Super capacitor-based energy storage - its analysis and simplified models:

7.4.2 Electric Double-Layer Capacitors

Compared to conventional capacitors, an EDLC has higher electrode surface area (2000 m^2/g), thinner and porous electrodes (smaller than 150 µm), and electrode micropores in the Angstrom order of magnitude. Unlike conventional capacitors that employ a solid dielectric material, the material between both electrodes in an EDLC is an electrolyte, and it can be either aqueous or organic based. Both the electrolyte solvent and any dissolved ions can be absorbed into the micropore structures. A separator is also present to separate the electrodes. Each part is depicted in Figure 7.13. An example of a microstructure is shown in Figure 7.14.

Energy is stored in an EDLC as charge separation, where the electrolyte ions diffuse toward the electrodes. This ion diffusion process in the electrolyte is similar to the one in electrochemical-based storage described in Section 7.3. The internal separation of charge by the movement of ions generates an internal electric field. Most of the energy is stored in the interface between the electrode and electrolyte, the so-called Helmholtz layer. It is sandwiched by two layers, one is the accumulated electrolyte ions, and the other is attracted charge in the electrode. The Helmholtz layer is typically in the order of one atom in thickness, which yields a large capacitance at the electrolyte/electrode interface. There are two Helmholtz layers in an EDLC, one at each positive/negative electrode. The mobility of the ions is effectively exploited to reduce as much as possible

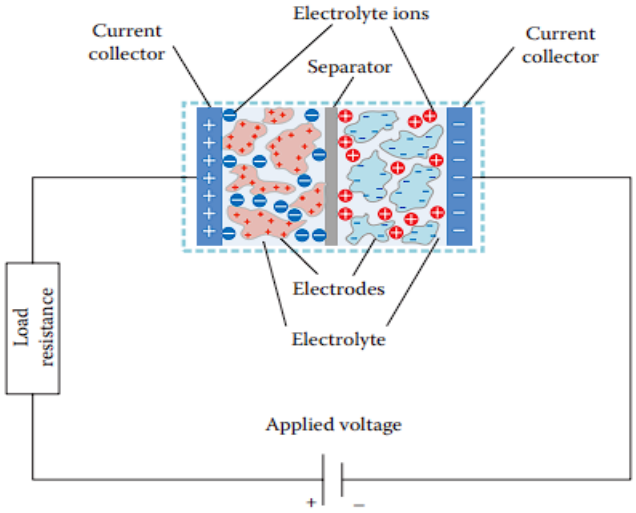

FIGURE 7.13 EDLC diagram.

the charge separation distance needed to increase capacitance. The amount of charge stored is further increased due to the high electrode surface and small micropore diameter. The energy storage mechanism for an EDLC is completely non-Faradaic. These ultracapacitors normally have carbon-based electrodes made from activated carbon or are constructed from carbon nanotubes/nanostructures. The electrolyte composition can vary from aqueous (H_2SO_4 or KOH) to organics such as acetonitrile. The main difference in terms of operation is in the equivalent series resistance (ESR) and pore size needed. Normally, aqueous-based electrolytes need smaller pore size and present a lower ESR. Organic electrolytes present a higher breakdown voltage. When voltage is applied, the electrolyte ions are separated, each being attracted by the electrode with opposite charge. This non-Faradaic energy storage is highly reversible, allowing EDLCs to reach million cycle lifetimes. The packaging styles can be similar to the cell packaging shown in Figure 7.9 to further increase power and energy density. The conceptual difference between EDLC and electrochemical storage is shown in Figure 7.15.

7.6.3 Ultracapacitor Cell

Compared to electrochemical cells, ultracapacitor cells exhibit less nonlinear behavior and can be modeled fairly well using equivalent circuit-based models. The simplest approach is to model the cell with an ideal capacitor element and an ESR to represent losses; this approach is depicted in Figure 7.19.

For an EDLC, the model can be decomposed to consider the different dominant parts of the ultracapacitor model in Figure 7.15 to obtain the equivalent circuit model in Figure 7.20. Ideal capacitors C_{HL1}, C_{HL2} can model the two capacitive Helmholtz dual layers at each electrode/electrolyte interface. In between these layers, a resistor R_{se} can model the ionic resistance due to the separator and movement through the electrolyte. An additional two resistances R_{e1}, R_{e2} can represent the electrical resistances at the electrode and cell terminal.

Transient and high-frequency responses can be modeled by adding inductor and RC elements, as depicted in Figure 7.21. This approach can be amenable to HCs since RC dynamics can be used to model transient behavior from Faradaic electrodes. Additional RC pairs can be added if necessary.

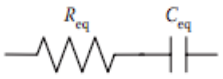

FIGURE 7.19 Series resistance ultracapacitor equivalent circuit model.

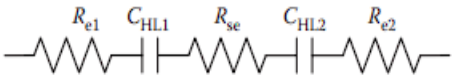

FIGURE 7.20 EDLC equivalent circuit model.

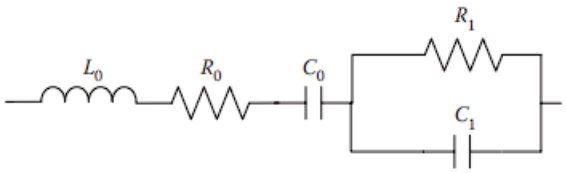

FIGURE 7.21 Ultracapacitor equivalent circuit model with inductor and RC dynamics.

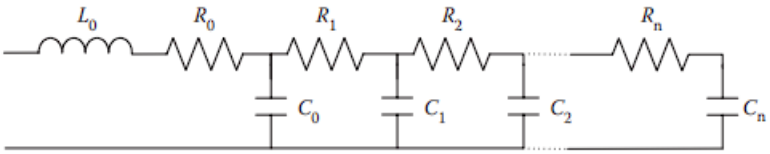

FIGURE 7.22 Multistage ladder model of ultracapacitor.

A multistage model depicted in Figure 7.22 is another common approach. It mimics the distributed physical nature of the ultracapacitor fairly well, for example, the large surface is at the porous electrode/electrolyte interface in an EDLC. This model has also been shown to fit empirical experimental data fairly well over a large frequency range. The number of stages or model order can be chosen based on the number of dominant time constants observed from experimental data. In an EDLC, effects such as ionic diffusion in the electrolyte and ion movement through macro/micro pores can occur at different timescales. An order selection of three or higher is commonplace.

4.Flywheels and their modelling for energy storage in EV/HEV:

10.3 Ultrahigh-Speed Flywheels

The use of flywheels for storing energy in mechanical form is not a new concept. More than 25 years ago, the Oerlikon Engineering Company in Switzerland made the first passenger bus solely powered by a massive flywheel. This flywheel, which weighed 1500 kg and operated at 3000 rpm, was recharged by electricity at each bus stop. The traditional flywheel is a massive steel rotor with hundreds of kilograms that spins on the order of ten hundreds of rpm. On the contrary, the advanced flywheel is a lightweight composite rotor with tens of kilograms and rotates on the order of 10,000 rpm; it is the so-called ultrahigh-speed flywheel.

The concept of ultrahigh-speed flywheels appears to be a feasible means for fulfilling the stringent energy storage requirements for EV and HEV applications, namely high specific energy, high specific power, long cycle life, high-energy efficiency, quick recharge, maintenance free characteristics, cost effectivenees, and environmental friendliness.

10.3.1 Operation Principles of Flywheels

A rotating flywheel stores energy in the kinetic form as

$$E_f = \frac{1}{2} J_f \omega_f^2 \tag{10.35}$$

where J_f is the moment of inertia of the flywheel in kgm^2/sec and ω_f is the angular velocity of the flywheel in rad/sec. Equation (10.32) indicates that enhancing the angular velocity of the flywheel is the key method of increasing its energy capacity and reducing its weight and volume. At present, a speed of over 60,000 rpm has been achieved in some prototypes.

With current technology, it is difficult to directly use the mechanical energy stored in a flywheel to propel a vehicle, due to the need for continuous variation transmission (CVT) with a wide gear ratio variation range. The commonly used approach is to couple an electric machine to the flywheel directly or through a transmission to constitute a so-called mechanical battery. The electric machine, functioning as the energy input and output port, converts the mechanical energy into electric energy or vice versa, as shown in Figure 10.14.

Equation (10.35) indicates that the energy stored in a flywheel is proportional to the moment of inertia of the flywheel and flywheel rotating speed squared. A lightweight flywheel should be designed to achieve moment of inertia per unit mass and per unit volume by properly designing its geometric shape. The moment of inertia of a flywheel can be calculated by

$$J_f = 2\pi\rho \int_{R_1}^{R_2} W(r) r^3 \, dr, \tag{10.36}$$

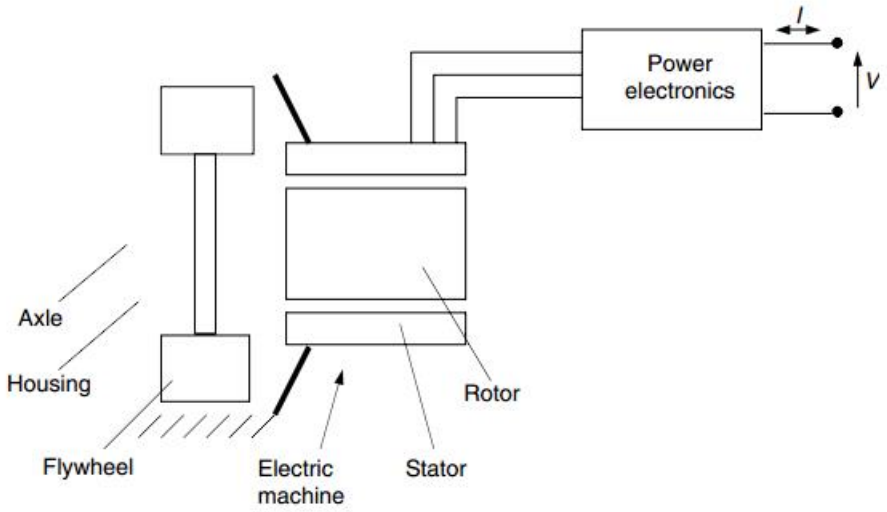

FIGURE 10.14
Basic structure of a typical flywheel system (mechanical battery)

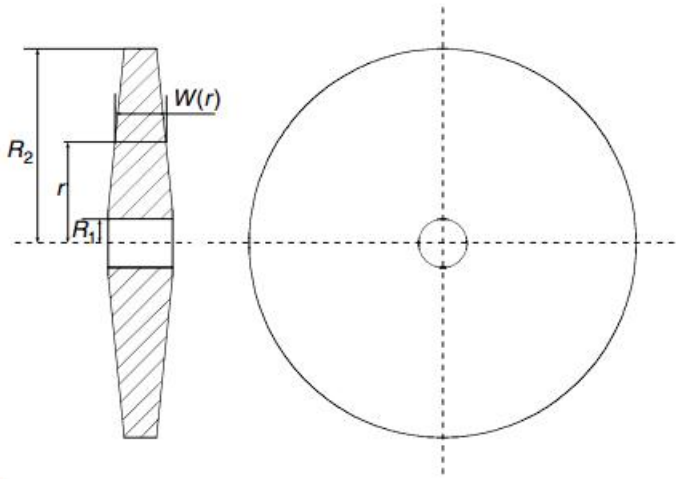

FIGURE 10.15
Geometry of a typical flywheel

where ρ is the material mass density and $W(r)$ is the width of the flywheel corresponding to the radius r, as shown in Figure 10.15. The mass of the flywheel can be calculated by

$$M_f = 2\pi\rho\int_{R_1}^{R_2} W(r) r\, dr. \tag{10.37}$$

Thus, the specific moment of inertia of a flywheel, defined as the moment of inertia per unit mass, can be expressed as

$$J_{fs} = \frac{\int_{R_1}^{R_2} W(r) r^3 \, dr}{\int_{R_1}^{R_2} W(r) r \, dr}. \tag{10.38}$$

Equation (10.35) indicates that the specific moment of inertia of a flywheel is independent of its material mass density and dependent solely on its geometric shape $W(r)$.

For a flywheel with equal width, the moment of inertia is

$$J_f = 2\pi\rho\left(R_2^4 - R_1^4\right) = 2\pi\rho\left(R_2^2 + R_1^2\right)\left(R_2^2 - R_1^2\right). \tag{10.39}$$

The specific moment of inertia is

$$J_{fs} = R_2^2 + R_1^2. \tag{10.40}$$

The volume density of the moment of inertia, defined as the moment of inertia per unit volume, is, indeed, associated with the mass density of the material. The volume of the flywheel can be obtained by

$$V_f = 2\pi \int_{R_2}^{R_2} W(r) r \, dr. \tag{10.41}$$

The volume density of the moment of inertia can be expressed as

$$J_{fV} = \frac{\rho \int_{R_1}^{R_2} W(r) r^3 \, dr}{\int_{R_1}^{R_2} W(r) r \, dr}. \tag{10.42}$$

For a flywheel with equal width, the volume density of the moment of inertia is

$$J_{fV} = \rho\left(R_2^2 + R_1^2\right). \tag{10.43}$$

Equations (10.42) and (10.43) indicate that heavy material can, indeed, reduce the volume of the flywheel with a given moment of inertia.

10.3.2 Power Capacity of Flywheel Systems

The power that a flywheel delivers or obtains can be obtained by differentiating equation (10.35) with respect to time, that is,

$$P_f = \frac{dE_f}{dt} = J_f \omega_f \frac{d\omega_f}{dt} = \omega_f T_f', \tag{10.44}$$

where T_f is the torque acting on the flywheel by the electric machine. When the flywheel discharges its energy, the electric machine acts as a generator and converts the mechanical energy of the flywheel into electric energy. On the other hand, when the flywheel is charged, the electric machine acts as a motor and converts electric energy into mechanical energy stored in the flywheel. Equation (10.44) indicates that the power capacity of a flywheel system depends completely on the power capacity of the electric machine.

An electric machine usually has the characteristics as shown in Figure 10.16, which has two distinct operating regions — constant torque and constant power region. In the constant torque region, the voltage of the electric machine is proportional to its angular velocity, and the magnetic flux in the air gap is constant. However, in the constant power region, the voltage is constant and the magnetic field is weakened with increasing machine angular velocity.

In charge of the flywheel, that is, accelerating the flywheel from a low speed, ω_0, to a high speed, maximum speed, ω_{max}, for example, the torque delivered from the electric machine is

$$T_m = J_f \frac{d\omega_f}{dt}, \tag{10.45}$$

where it is supposed that the electric machine is directly connected to the flywheel. The time, t, needed can be expressed as

$$t = \int_{\omega_0}^{\omega_{max}} \frac{J_f}{T_m} d\omega = \int_{\omega_0}^{\omega_b} \frac{J_f}{p_m/\omega_b}\omega + \int_{\omega_b}^{\omega_{max}} \frac{J_f}{p_m/\omega} d\omega. \tag{10.46}$$

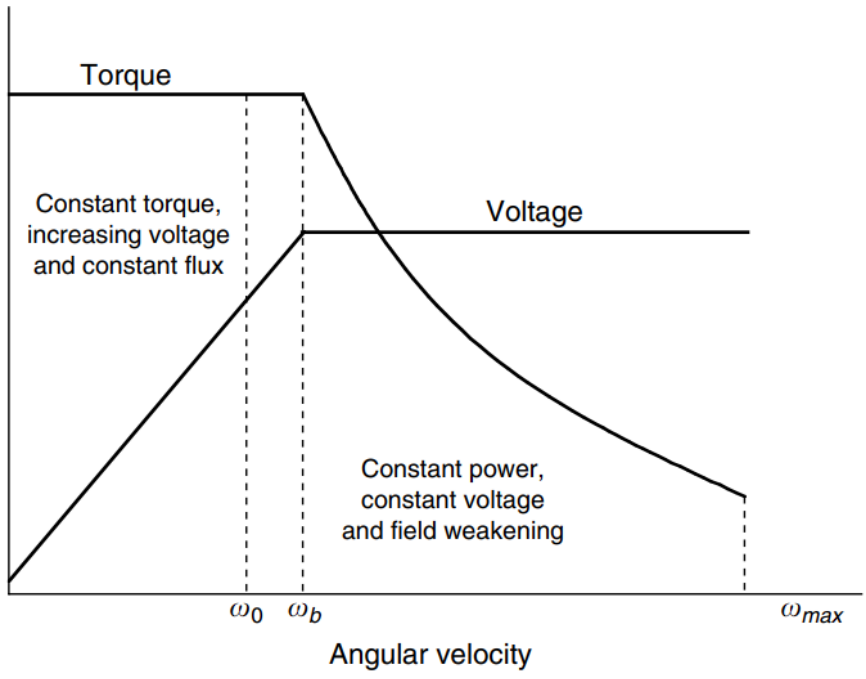

FIGURE 10.16
Typical torque and voltage profile vs. rotational speed

With the given accelerating time, t, the maximum power of the electric machine can be obtained from (10.46) as

$$P_m = \frac{J_f}{2_t}\left(\omega_b^2 - 2\omega_0\omega_b + \omega_{max}^2\right). \tag{10.47}$$

Equation (10.47) indicates that the power of the electric machine can be minimized by the design of its corner speed or base speed, ω_b, equal to the bottom speed of the flywheel, ω_0. This conclusion implies that the effective operating speed range of the flywheel should coincide with the constant speed region of the electric machine. The power of the electric machine can be minimized as

$$P_m = \frac{J_f}{2_t}\left(\omega_0^2 + \omega_{max}^2\right). \tag{10.48}$$

Another advantage achieved by coinciding the operating speed range of the flywheel with the constant power speed range is that the voltage of the electric machine is always constant (refer to Figure 10.16), therefore significantly simplifying the power management system, such as DC/DC converters and their controls.

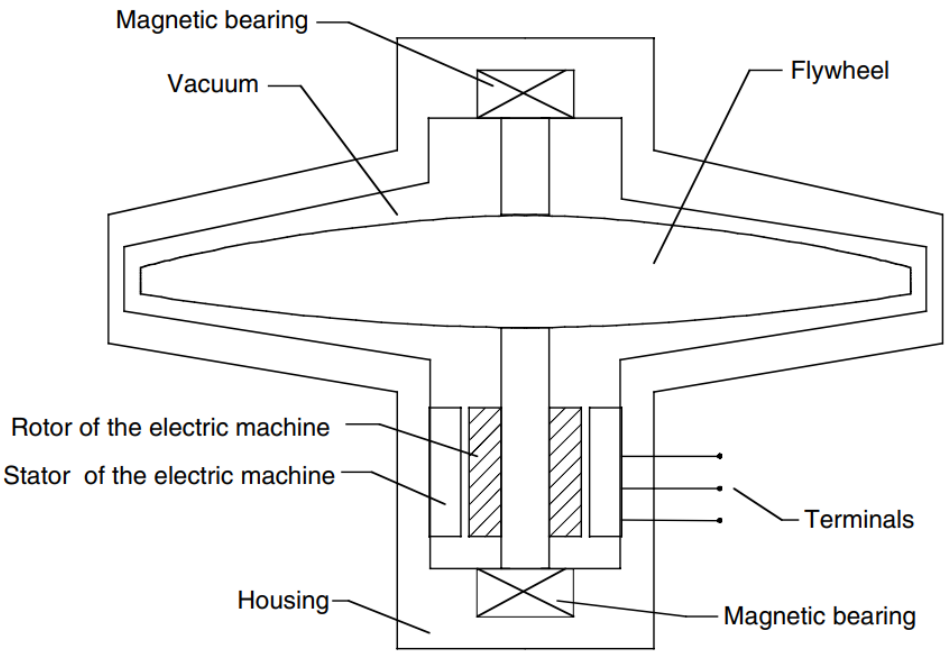

FIGURE 10.17
Basic structure of a typical flywheel system

5.Hybridization of various energy storage devices:

10.4 Hybridization of Energy Storages

The hybridization of energy storage is to combine two or more energy storages together so that the advantages of each one can be brought out and the disadvantages can be compensated by others. For instance, the hybridization of a chemical battery with an ultracapacitor can overcome such problems as low specific power of electrochemical batteries and low specific energy of ultracapacitors, therefore achieving high specific energy and high specific power.

Basically, the hybridized energy storage consists of two basic energy storages: one with high specific energy and the other with high specific power. The basic operation of this system is illustrated in Figure 10.18. In high power demand operations, such as acceleration and hill climbing, both basic energy storages deliver their power to the load as shown in Figure 10.18(a). On the other hand, in low power demand operation, such as constant speed cruising operations, the high specific energy storage will deliver its power to the load and charge the high specific power storage to recover its charge lost during high power demand operation, as shown in Figure 10.18(b). In regenerative braking operations, the peak power will be absorbed by the high specific

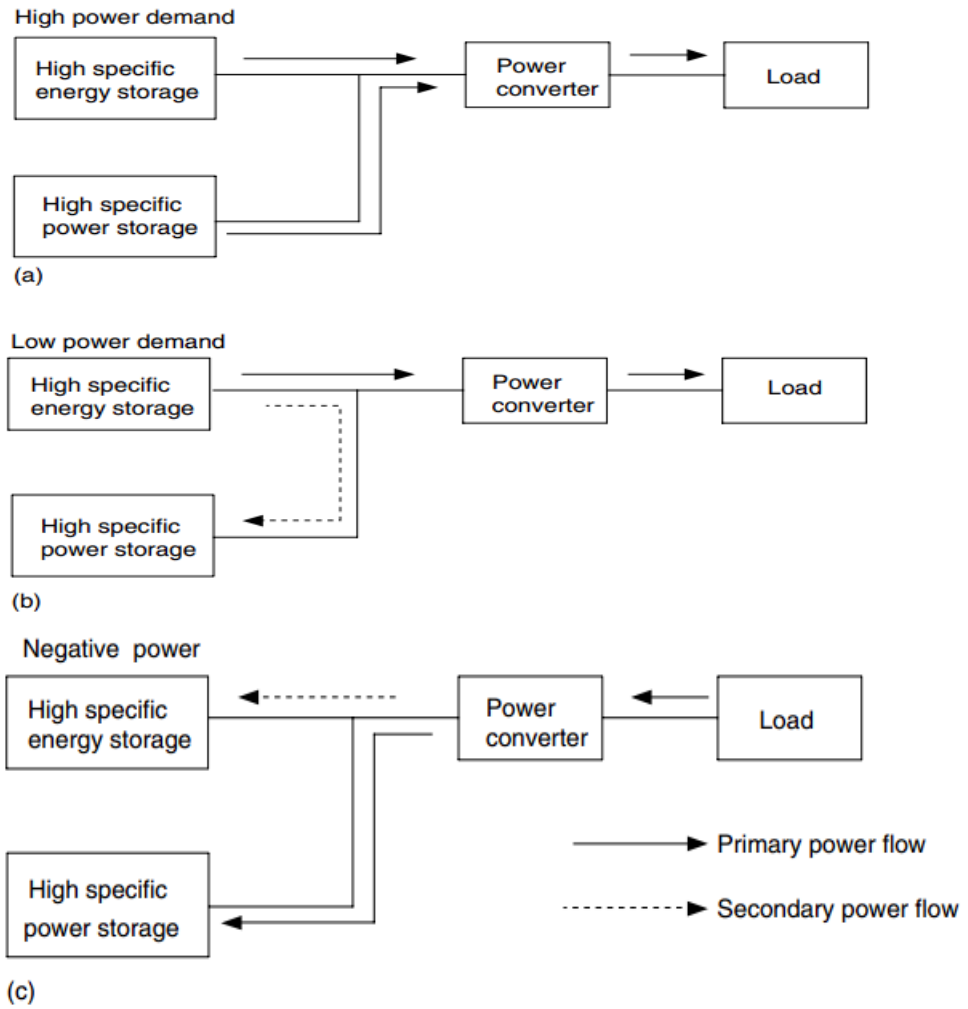

FIGURE 10.18
Concept of a hybrid energy storage operation

power storage, and only a limited part is absorbed by the high specific energy storage. In this way, the whole system would be much smaller in weight and size than if any one of them alone was the energy storage.

Based on the available technologies of various energy storages, there are several viable hybridization schemes for EVs and HEVs, typically, battery and battery hybrids, and battery and ultracapacitor hybrids. The latter is more natural since the ultracapacitor can offer much higher power than batteries, and it collaborates with various batteries to form the battery and ultracapacitor hybrids. During hybridization, the simplest way is to connect the ultracapacitors to the batteries directly and in parallel, as shown in Figure 10.19.

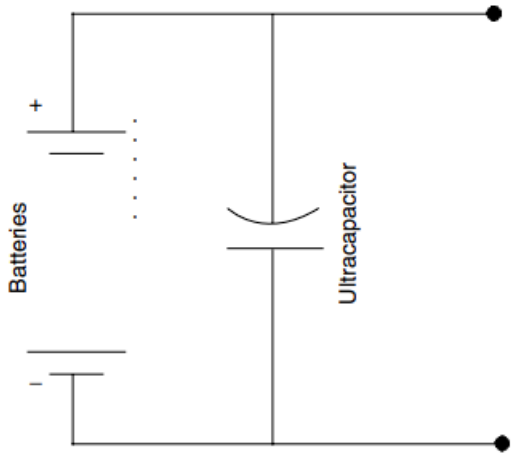

FIGURE 10.19
Direct and parallel connection of batteries and ultracapacitors

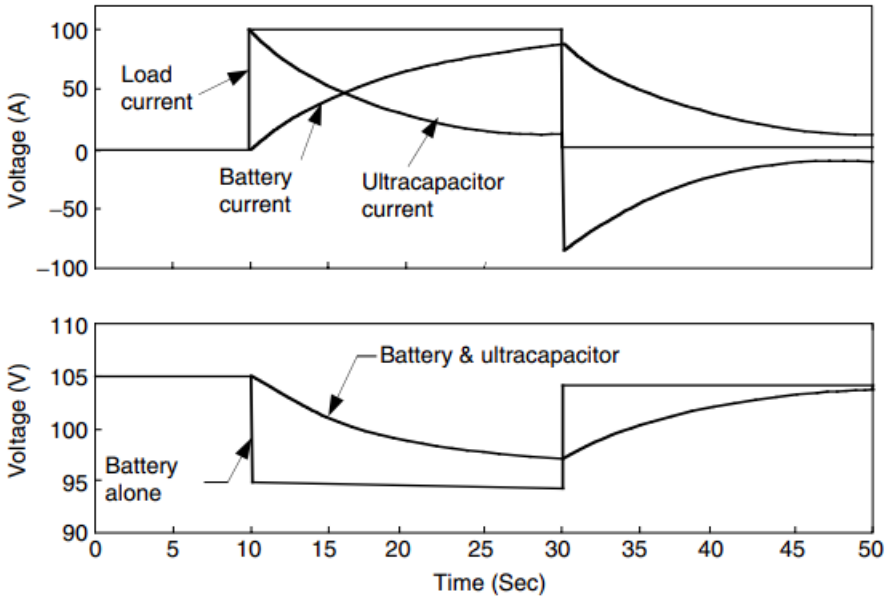

FIGURE 10.20
Variation of battery and ultracapacitor currents and voltages with a step current output change

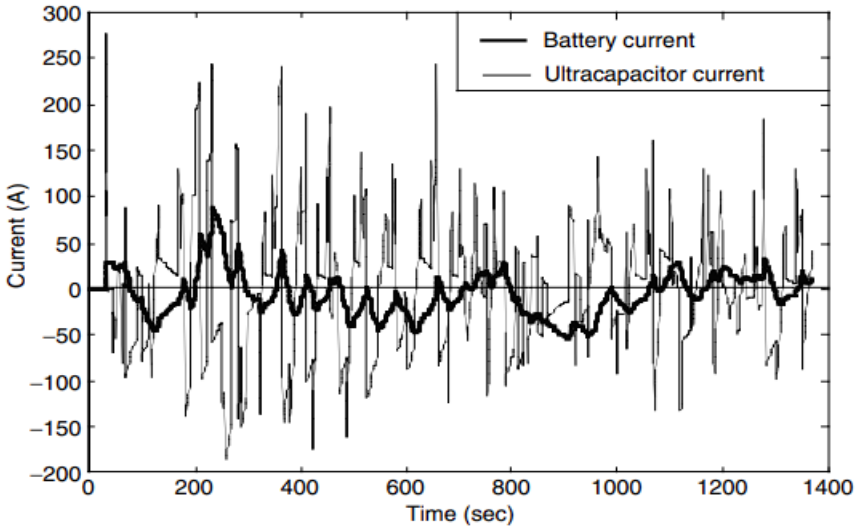

FIGURE 10.21
Battery and ultracapacitor currents during operation of HEV in an FTP 75 urban drive cycle

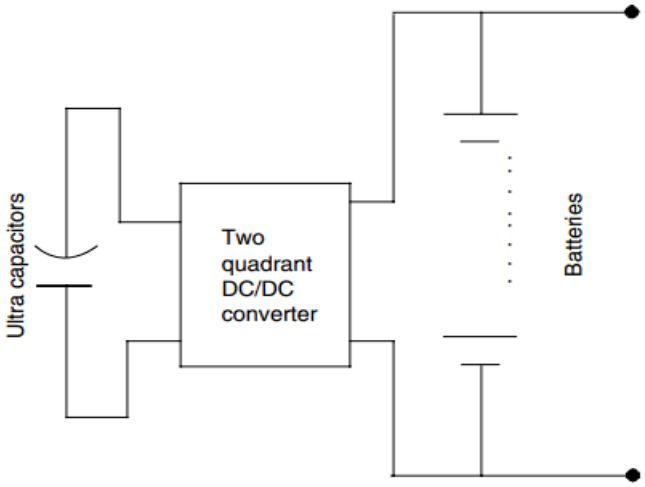

FIGURE 10.22
Actively controlled hybrid battery/ultracapacitor energy storage

In this configuration, the ultracapacitors simply act as a current filter, which can significantly level the peak current of the batteries and reduce the battery voltage drop as shown in Figure 10.20 and Figure 10.21. The major disadvantages of this configuration are that the power flow cannot be actively controlled and the ultracapacitor energy cannot be fully used.

Figure 10.22 shows a configuration in which a two-quadrant DC/DC converter is placed between the batteries and ultracapacitors. This design allows the batteries and the ultracapacitors to have a different voltage, the power flow between them can be actively controlled, and the energy in the ultracapacitors can be fully used. In the long term, an ultrahigh-speed flywheel would replace the batteries in hybrid energy storage to obtain a high-efficiency, compact, and long-life storage system for EVs and HEVs.